Understanding the seismic disorder attribute and its applications

Satinder Chopra[+] and Kurt J. Marfurt[†]*

[+]Arcis Seismic Solutions, Calgary; [†]The University of Oklahoma, Norman

Summary

While reflections associated with conformal sedimentary layers are usually coherent and continuous, other reflections such as mass transport complexes, karst collapse, and salt, may appear to be quite chaotic, without any specific orientation. We may also see chaotic events that have little to do with the target geology, but rather are artifacts due to variations in the overburden and surface or budget limitations resulting in a suboptimum acquisition program. While some of these artifact issues can be handled at the time of processing, a certain level of randomness remains in most seismic data volumes. Geologic features of interpretational interest such as fault damage zones, unconformities, and gas chimneys often have randomness associated with them, which can be characterized in terms of seismic disorder attribute amongst others.

We demonstrate the application of seismic disorder attribute to two different datasets and find that it is a useful attribute for assessing the signal-to-noise ratio and data quality, in addition to helping delineate damage zones associated with large faults, and the interior of salt dome structures.

Introduction

Seismic data interpretation is based on the identification and geologic classification of seismic amplitude and reflector morphology. The morphology in stratigraphic interpretation include the identification of conformal, onlapping, offlapping, hummocky, and chaotic reflector packages, ideally integrated within a sequence stratigraphic framework. In addition to the seismic reflections corresponding to simple stratigraphic deposition, tectonic deformation, or hydrocarbon accumulation, we often encounter seismic reflections that change abruptly in different directions, exhibiting no specific waveform shape, amplitude or orientation. Such data configurations are referred to as *seismic disorder*, *randomness* or *chaos*, which can represent either seismic or geologic noise, or a combination of the two. Seismic noise that can be an indicator of the underlying geology include salt domes where the internal reflectivity is anomalously low and overprinted by random seismic noise, and gas chimneys and overpressured zones where an inaccurate velocity results in suboptimum imaging. The seismic "disorder" attribute measures all of these phenomena, and can provide either geologic insight or quantify the amount of seismic noise in the data, which may be useful in subsequent risk analysis

In some early attempts at studying randomness as it pertains to noise, Dash and Obaidullah (1970) described a crosscorrelation method for determination of signal and noise statistics for two seismic traces. This means of estimating the coherent component of the seismic data is used by several interpretation software packages as input to subsequent spectral balancing operations. Crosscorrelation was used by the deep crustal reflection seismology community to highlight the rather infrequent coherent reflectors. This technique also formed the basis of highlighting discontinuities in exploration seismic data leading to the first coherence attribute (Bahorich and Farmer, 1995).

Randen et al. (2001) introduced the chaos attribute that is based on the eigenanalysis of the 3x3 gradient structure tensor. If the first eigenvalue is large, the corresponding first eigenvector defines the normal to a local plane of constant amplitude waveforms. If the three eigenvalues are equal, the data are totally chaotic. Intermediate values of chaos indicate the degree of data organization. The chaos attribute is available in several commercial software packages.

A totally different approach to quantifying randomness is through the use of the grey-level cooccurrence matrix (GLCM) texture attributes (West et al., 2002; Gao, 2003; Chopra and Alexeev, 2005). The cooccurrence matrix is computed from a structurally aligned window of seismic amplitude, and can measure both organized (linear, wavy, brick) and disorganized patterns. Specifically, the GLCM entropy attribute describes the degree of disorder in the data and yields large values for chaotic or noisy regions in the seismic data.

Al-Dossary et al. (2014), proposed the seismic disorder attribute, which is sensitive to chaotic reflection patterns and noisy areas, and relatively insensitive to more organized discontinuities such as faults and channel edges. The algorithm essentially cascades a second derivative in the inline, crossline and time directions on a window of the computed power (or energy) of the data. This is equivalent to squaring the data and filtering it with a disorder filter given as

$$\mathbf{L} = \left\{ \begin{bmatrix} 1 & -2 & 1 \\ -2 & 4 & -2 \\ 1 & -2 & 1 \end{bmatrix}, \begin{bmatrix} -2 & 4 & -2 \\ 4 & -8 & 4 \\ -2 & 4 & -2 \end{bmatrix}, \begin{bmatrix} 1 & -2 & 1 \\ -2 & 4 & -2 \\ 1 & -2 & 1 \end{bmatrix} \right\} \qquad (1)$$

The application of this algorithm to seismic data has two drawbacks in that it is sensitive to local average amplitude yielding low disorder values for chaotic zones with low amplitude, and exhibits some dubious diagonal lines (Al-Dossary et al., 2014). Ha and Marfurt (2014) modified the algorithm by dividing the seismic disorder attribute by the RMS amplitude of the windowed data such that now it can be written as

$$Disorder = \frac{\mathbf{L}.\mathbf{e}}{|\mathbf{L}| * |\mathbf{e}| + \varepsilon},$$

where **L** is defined in equation 1, **e** is a cube of amplitude energy, '**.**' indicates a triple inner product, $|\quad|$ indicates RMS magnitude

and ε is a small additive constant that prevents division by zero in the computations. When the seismic disorder attribute is computed along structural dip, the diagonal artifact is minimized. We show applications of the seismic disorder attribute to different types of features seen in 3D seismic data volumes and demonstrate the insight that can be gained therefrom.

Applications: Example 1

Our first example is a vertical slice through a good quality 3D seismic volume acquired in northwest Alberta, Canada showing three picked reflectors (Figure 1). At the location of the fault indicated by yellow arrows, we expect the reflection amplitudes to be coherent with a single discontinuity for a simple fault, and incoherent if there is a somewhat wider damage zone representing a suite of conjugate faults. At the shallower horizons above this fault, marked with magenta and blue arrows, we see more continuous reflectors that drape or flex over the deeper fault. Just above each of these two horizons, it may be difficult to assess the disorder or entropy in the data. In Figures 2 and 3 we exhibit the corresponding images through the entropy and disorder attribute volumes. At the location of the fault (yellow arrows), the entropy is seen to be high as expected. In the regions 40 ms above horizons 1 and 2 marked by magenta and blue arrows, the entropy and disorder values are also higher, due to the lower coherency of the reflections. However, notice that the disorder attribute shows more distinct variation at these locations, as highlighted by the yellow hexagon. The seismic disorder attribute seems to convey information that is more easily interpretable.

In Figure 4a, we show a chair display with a vertical section through the seismic amplitude data and a strata slab through the seismic disorder attribute. Notice that the disorder attribute values along the horizon, i.e. along the top of the strata slab are all low as the horizon is quite smooth. At the location of the yellow arrow, we notice a streak of higher disorder attribute values. This streak corresponds to the hypothesized damage zone seen at a lower level in Figures 1 to 3.

Figure 4b shows the same data as in Figure 4, but now at a stratal slice at the top of the yellow horizon. Higher disorder values are clustered about the fault, suggesting a thinner damage zone. If we look at the equivalent chair display in Figure 4c, where the vertical section is now through the seismic amplitude volume, there is a sharp reflector displacement across the fault. But just below this level we see higher values of the disorder attribute on both sides of the fault. We interpret these higher disorder values to be indicative of a damage zone associated with the main fault, but we need to evaluate the alternative hypothesis that the data are simply contaminated by noise.

Preconditioning of seismic data and the seismic disorder attribute

In addition to computing attributes on the original data, we advise that the interpreter repeat the computation on the data after preconditioning. Common poststack data conditioning processes include enhancing the signal-to-noise ratio and sharpening the discontinuities (Chopra and Marfurt, 2008), spectrally balancing or even boosting the frequency content of the data (Chopra et al., 2011), while less common prestack data conditioning processing include interpolating missing traces, regularizing the offset and azimuth geometry (Chopra and Marfurt, 2013), and suppressing the acquisition footprint. Such processing of the seismic data often helps obtain better quality attributes and which can lead to more meaningful interpretation. The interpreter should always compare the seismic data before and after such data conditioning to make sure that more chaotic features of geologic interest are retained.

In Figures 5a and b we show strata slices through the disorder attribute before and after structure-oriented filtering. Notice the enhanced signal-to-noise ratio as well as the sharpness of the faults after preconditioning. The energy ratio coherence attribute (seen in black) using transparency is overlaid on the displays. We see the coherence lineaments exactly overlaying the fault indicated as at A. However, the faults indicated at B and C have higher disorder values seen on both sides of the black coherence lineaments. We interpret such values as being indicative of fractures associated with the main faults with confidence.

Example 2: The next example is from a prestack depth migrated data volume acquired in the Gulf of Mexico. Equivalent vertical slices are shown in Figure 6 through the seismic amplitude, disorder and energy volumes. While a prominent salt dome is seen in the middle of the sections, notice that the outline of the salt body is not well defined everywhere, but can be easily interpreted using concepts of pattern recognition that differentiate the seismic response inside the salt dome from that outside (Figure 6a and b).

Just outside the interpreted salt outline on the left and right of the dome, the seismic reflections are insufficiently imaged, and appear as broken, somewhat chaotic, but relatively strong amplitude events highlighted by the orange, magenta, yellow and cyan polygons. Accordingly, the disorder attribute points out higher values in these highlighted areas. In contrast, the chaotic (mostly noise) events inside the salt dome are lower in amplitude. In order to differentiate the two chaotic patterns, we need to add a second attribute (energy) that is sensitive to the strength of these chaotic events (Figure 6c). A geobody can then be picked by corendering the two images. In a similar way, the seismic disorder attribute can be used to map incoherent reflection packages such as mass transport complexes and karst collapse features.

Conclusions

We have shown the application of seismic disorder attribute to two different data examples and have found that it is a useful attribute. By construction, the disorder attribute has a low response to sharp faults and coherent reflectors, but a higher response to more diffuse fault zones and incoherent reflectors. Structure-oriented filtering appears to enhance these damage zones. More quantitative assessment of such images will require horizontal image logs through diverse fault zones

Acknowledgements: We thanks Arcis Seismic Solutions, TGS, Calgary, for permission to present this work.

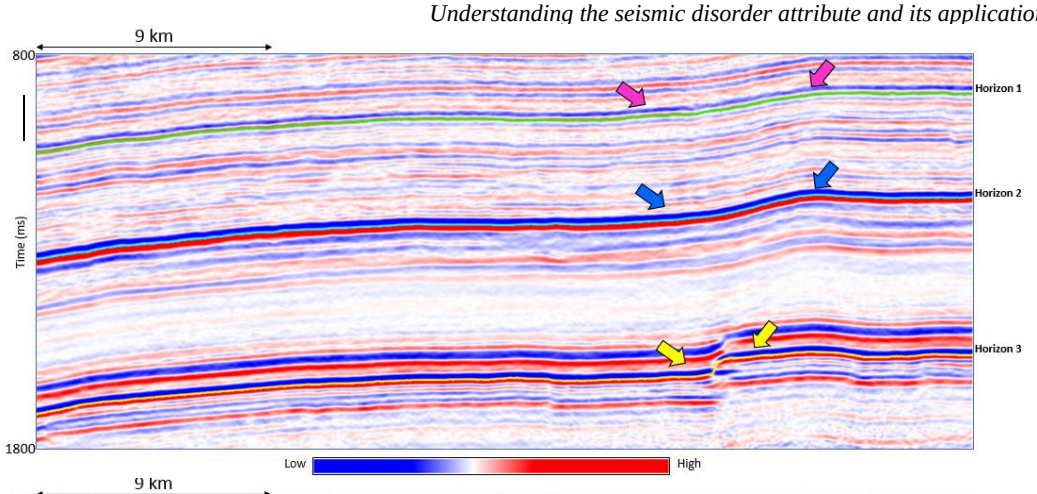

Figure 1: A segment of the inline from a 3D seismic volume. At the location of the fault indicated with yellow arrows, the seismic amplitudes are not expected to be coherent. At the location of the blue and magenta arrows, just above the horizons, it may be difficult to ascertain the disorder or the entropy. *(Data courtesy: Arcis Seismic Solutions, TGS, Calgary)*

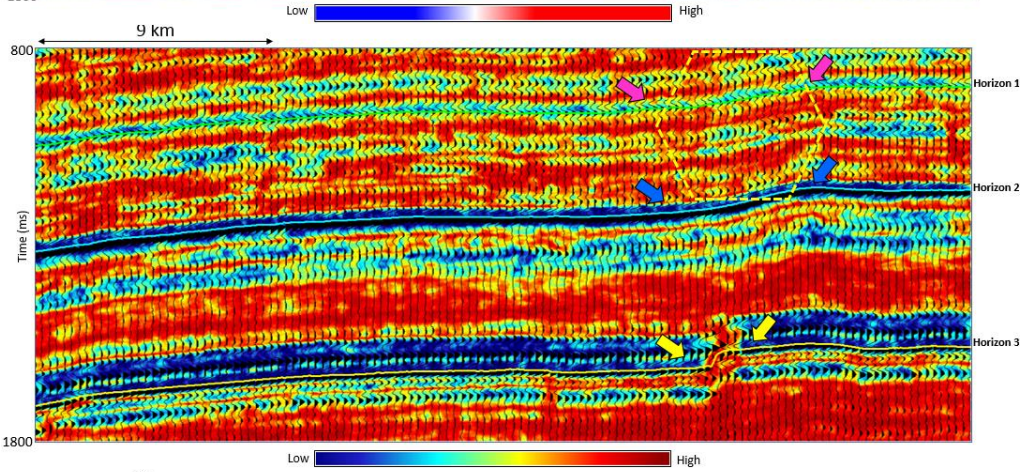

Figure 2: The same segment of the inline from a 3D seismic volume as shown in the previous slide displays in wiggle and variable area overlaid on equivalent section from the entropy volume. Higher values of disorder are shown in bright orange. At the location of the fault indicated with yellow arrows, the entropy is quite high as expected. At the location of the blue and magenta arrows, just above the horizons, the entropy is higher and is open for interpretation. Every fourth trace has been plotted for the seismic data overlay. *(Data courtesy: Arcis Seismic Solutions, TGS, Calgary)*

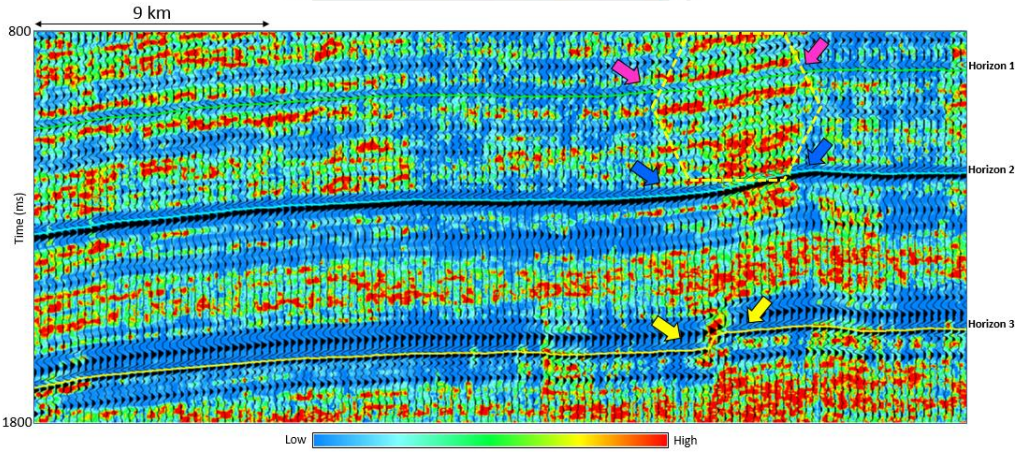

Figure 3: The same segment of the inline from a 3D seismic volume as shown in the Figure 1 displays in wiggle and variable area overlaid on equivalent section from the disorder volume. Higher values of disorder are shown in bright orange. At the location of the fault indicated with yellow arrows, the disorder is quite high as expected. At the location of the blue and magenta arrows, just above the horizons, the disorder is higher and is open for interpretation. Every fourth trace has been plotted for both the seismic. *(Data courtesy: Arcis Seismic Solutions, TGS, Calgary)*

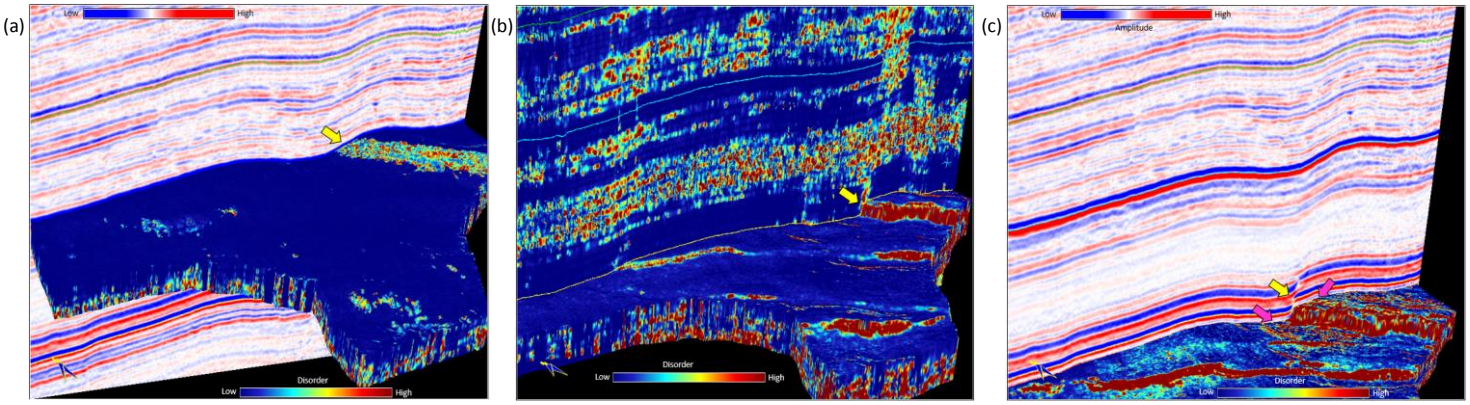

Figure 4: shows chair displays with the horizontal sections as strata cubes from the disorder volume at different levels and the vertical sections from the seismic volume (in a and c) and the disorder volume (in b). At the location of the blue arrows in Figure 1, the horizon is coherent and thus leads to a good horizon pick. In (a) the disorder attribute values are all low, except at the dipping zone indicated with the yellow arrow. At the location of the yellow arrows in Figure 1, the horizon is coherent everywhere except at the location of the fault, and thus in Figure 1b we see high disorder attribute values only at the fault. A few milliseconds below the yellow horizon as seen in the strata-cube in Figure (c) the disorder attribute values are all low elsewhere, except at the fault and a small width about both sides of the fault and indicated with the magenta arrows. *(Data courtesy: Arcis Seismic Solutions, TGS, Calgary)*

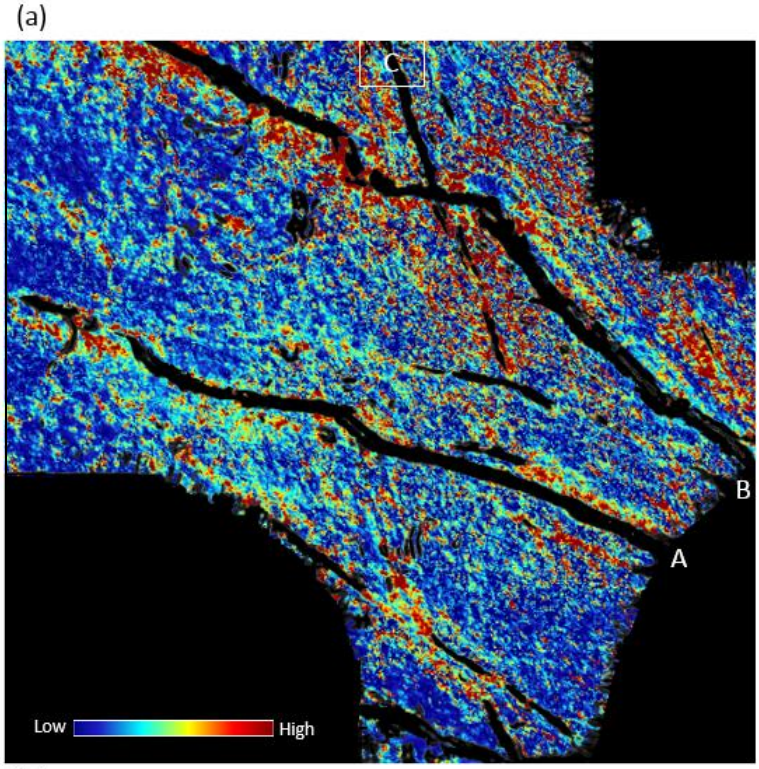

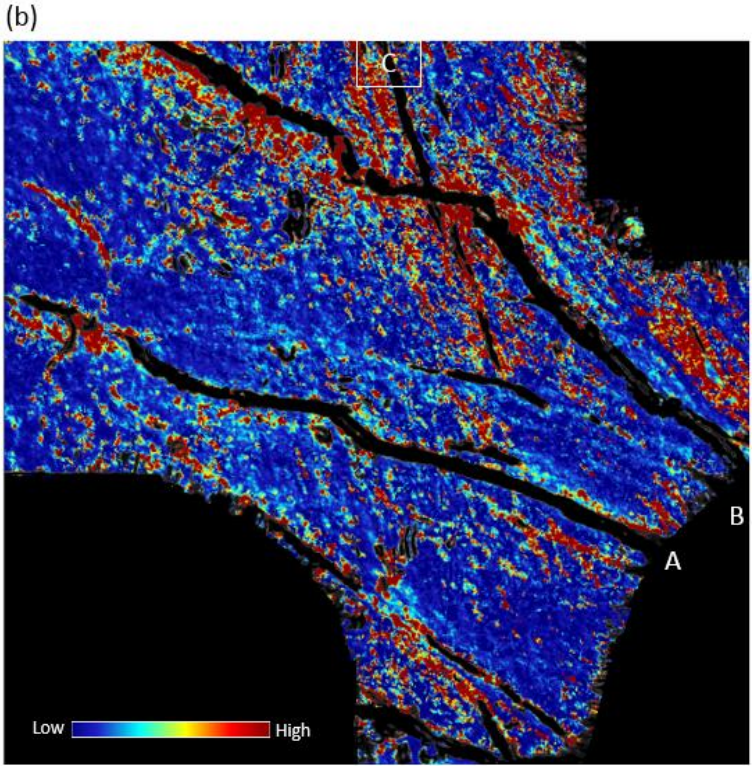

Figure 5: Strata-slices 72ms below a marker horizon close to 1600ms from (a) disorder run on input seismic data, and (b) from input seismic data after preconditioning. The coherence attribute has been overlaid (in black) on the two displays using transparency. Notice the low disorder values in the background and enhanced disorder lineaments indicating faults. *(Data courtesy: Arcis Seismic Solutions, TGS, Calgary)*

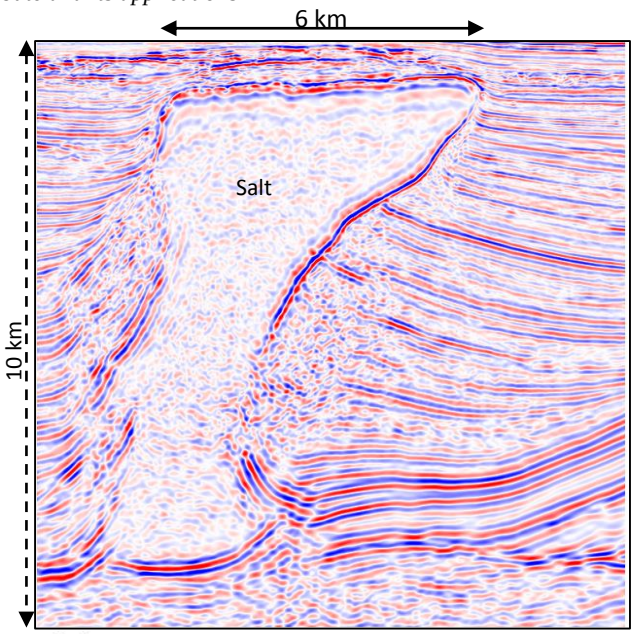

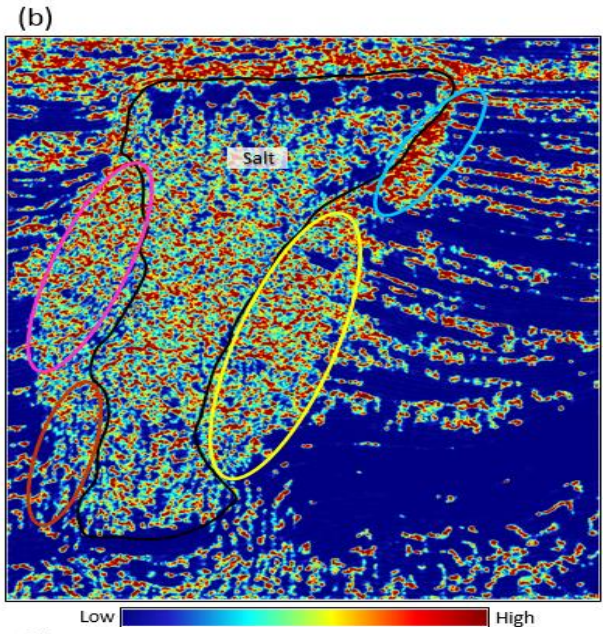

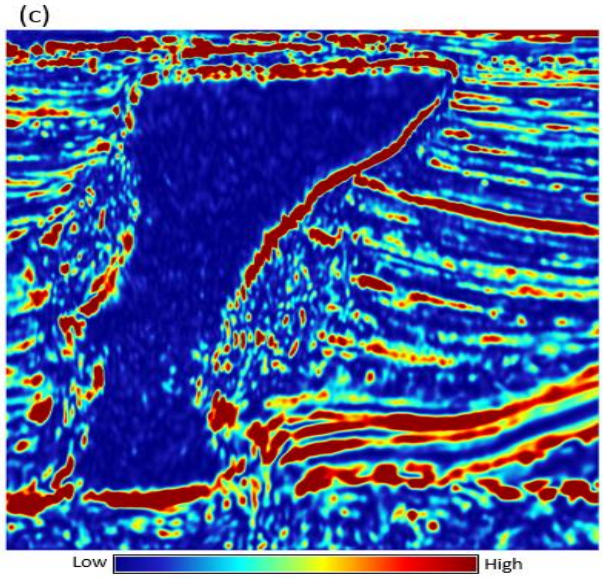

Figure 6: Segment of (a) a seismic depth section (a) with interpretation from the Gulf of Mexico showing a massive salt dome. The boundary of the dome is well-defined on the right, but on the left all we see are the abutting reflections. The body of the salt exhibits low amplitude chaotic reflections, while the poorly imaged chaotic reflectors outside the salt dome are high amplitude. The equivalent depth section in (b) shows the disorder attribute, and in (c) the energy attribute within a 50 m by 50m by 50 m window. The body of the salt, as well as the areas in the highlighting ellipses exhibits low energy chaotic reflections which are can be distinguished from the high-energy chaotic reflections outside the interpreted salt body. *(Data courtesy: TGS, Houston)*

EDITED REFERENCES

Note: This reference list is a copyedited version of the reference list submitted by the author. Reference lists for the 2016 SEG Technical Program Expanded Abstracts have been copyedited so that references provided with the online metadata for each paper will achieve a high degree of linking to cited sources that appear on the Web.

REFERENCES

Al-Dossary, S., Y. E. Wang, and M. McFarlane, 2014, Estimating randomness using seismic disorder: Interpretation (Tulsa), **2**, SA93–SA97, http://dx.doi.org/10.1190/INT-2013-0088.1.

Bahorich, M., and S. Farmer, 1995, 3-D seismic discontinuity for faults and stratigraphic features: The coherence cube: The Leading Edge, **14**, 1053–1058, http://dx.doi.org/10.1190/1.1437077.

Chopra, S., and V. Alexeev, 2005, Applications of texture attributes to 3D seismic data: CSEG Recorder, **30**, 28–32.

Chopra, S., and K. J. Marfurt, 2008, Gleaning meaningful information from seismic attributes: First Break, **26**, 43–53, http://dx.doi.org/10.3997/1365-2397.2008012.

Chopra, S., and K. J. Marfurt, 2013, Preconditioning seismic data with 5D interpolation for computing geometric attributes: The Leading Edge, **32**, 1456–1460, http://dx.doi.org/10.1190/tle32121456.1.

Chopra, S., S. Misra, and K. J. Marfurt, 2011, Coherence and curvature attributes on preconditioned seismic data: The Leading Edge, **30**, 386–393, http://dx.doi.org/10.1190/1.3575281.

Dash, B. P., and K. A. Obaidullah, 1970, Determination of signal and noise statistics using correlation theory: Geophysics, **35**, 24–32, http://dx.doi.org/10.1190/1.1440077.

Gao, D., 2003, Volume texture extraction for 3-D seismic visualization and interpretation: Geophysics, **68**, 1294–1302, http://dx.doi.org/10.1190/1.1598122.

Gersztenkorn, A., and K. J. Marfurt, 1999, Eigen structure-based coherence computations as an aid to 3Dstructural and stratigraphic mapping: Geophysics, **64**, 1468–1479, http://dx.doi.org/10.1190/1.1444651.

Ha, T., and K. J. Marfurt, 2014, Disorder attribute implementation on TX-LA dataset: Estimate horizon-picking confidence and map chaotic features, The University of Oklahoma, AASPI Annual Meeting.

West, B., S. May, J. E. Eastwood, and C. Rossen, 2002, Interactive seismic facies classification using textural attributes and neural networks: The Leading Edge, **21**, 1042–1049, http://dx.doi.org/10.1190/1.1518444.